Electron Channeling in Si, Ag, and Au Crystals

S. Kjaer Andersen, F. Bell,* F. Frandsen, and E. Uggerhøj†
Institute of Physics, University of Aarhus, DK-8000 Aarhus C, Denmark
(Received 9 February 1973)

Electron-channeling experiments have been performed on Si, Ag, and Au single crystals with energies between 0.5 and 3 MeV, using the Rutherford scattering technique. The influence of multiple scattering was studied by varying the target thickness. The results are discussed within the framework of the dynamical theory of diffraction and Lindhard's classical model. Quantitative measurements on the reciprocity theorem reveal that it is possible to link the enhancement in Rutherford scattering yields with Kikuchi defect bands in the forward direction. This connection can be described quantitatively by a recent Kikuchi-band theory.

I. INTRODUCTION

Channeling of heavy particles (protons, α particles, etc.) has been investigated in great detail. Such directional effects have in the past proved to be powerful tools for the investigation of the surface of solids, radiation damage in single crystals and its annealing behavior; furthermore, the effects have been used to locate foreign atoms in crystals (for a review, see Ref. 1). The basic theoretical description of these directional effects has been given by Lindhard,[2,3] and the experimental results are found to be in good agreement with theory.

Lindhard[2] showed that the probability for penetration to the center of strings is small (~ 1–2%) for aligned positrons with energies exceeding ~ 1 MeV, so that one would expect nearly the same directional effects for protons and positrons. This fact was the motivation for the investigation of channeling effects for positrons. The basic features were shown in Ref. 4, where the angular distribution of electrons and positrons emitted from ^{64}Cu embedded in copper single crystals was studied simultaneously. It was observed that the positrons show very pronounced dips in yield whenever they are emitted within a certain critical angle around an axial or planar direction. Conversely, for the electrons, a very pronounced peak in yield was found around an axial or planar direction. The results were found to be in fair agreement with estimates based upon classical mechanics.

A more precise way of investigating such channeling effects is to inject an external electron or positron beam and measure wide-angle Rutherford scattering, because radiation damage is created by the implantation in the above emission experiments. But unfortunately, for well-defined scattering depths, thin crystalline foils are needed.

Wide-angle Rutherford scattering with positrons has been studied in thin gold[5] and silicon[6] crystals. As shown by Lervig *et al.*,[3] the positrons are expected to behave nearly classically, so the dips in scattering yield for positrons and protons should be nearly identical. Experiments show that this is indeed the case, apart from a small difference in minimum yield, which may be ascribed to scattering by electrons. Hence there is no experimental evidence for an appreciable tunneling of positrons into classically forbidden regions.

In general, the behavior of electrons is quite different from that of positrons. While positrons are seen to behave like protons, being pushed away from the atomic strings, electrons can usually move everywhere in the lattice, but may also be trapped in the potential holes around the strings. The possibility of electrons moving in bound states along the crystal axis, described by classical mechanics, has been studied theoretically by Lindhard,[7] Bell *et al.*,[8] and Nip and Kelly.[9] The fact that the experimental channeling effects for positrons and electrons were related to descriptions based upon classical mechanics was met with strong criticism from people working with diffraction calculations.[10] De Wames *et al.*[11] pointed out that electron and positron channeling should be understood on the basis of the diffraction theory. Also, Howie[12] has made calculations on the basis of diffraction theory. The discussion initiated further theoretical and experimental investigations. For a general review of electron-channeling theories based upon the dynamical theory of electron diffraction, see Ref. 13. Howie *et al.*[14] have investigated electron channeling and compared the experimental results with classical calculations as well as with calculations based upon the diffraction theory, and Andersen *et al.*[15] have investigated electron channeling in Si crystals and compared the results with both classical and quantal descriptions.

In a previous paper,[16] axial and planar channeling of fast electrons in gold single crystals was investigated, and the experimental results com-

pared with Lindhard's theory.[7] He discusses the quantities that discern between a classical and a quantal description and points out that when the number ν of bound states in the transverse phase space is large, the classical approximation may be favorable. It was found in Ref. 16 that the axial-channeling effects for electrons (~ 1 MeV) on gold crystals could be reasonably well described on the basis of Lindhard's theory.

In order to provide a more general picture of electron channeling, further experiments have been performed with electron energies from 600 keV to 3 MeV and with different kinds of single crystals.

The Rutherford scattering yield is measured as a function of the angle between the incident beam and the axial (planar) directions in the crystals. The results are compared with calculations based upon the diffraction theory as well as with classical calculations and thus, direct information about the applicability of a classical description is obtained. Furthermore, the rule of reversibility (reciprocity) is investigated and found to hold. From the distribution of electrons around the forward direction, a connection between channeling effects and Kikuchi bands is discussed.

II. EXPERIMENTAL PROCEDURE

Figure 1 shows the experimental setup. A beam of electrons is obtained from either the 2-MV or the 5-MV Van de Graaff at Aarhus University. Both facilities are equipped with a new charging system, designed by Miller and co-workers.[17] It is located in the terminal of the accelerator so that the machine operates at both polarities with the same ripple in the voltage. In the present experiments, the ripple was $\lesssim$ 1 kV, which made it possible to have a stable electron beam through a magnet (field stability ~ 10^{-5}), even with a beam divergence of 0.03°. The voltage stabilization was provided by a refined generating voltmeter and a feedback system to the charging device. In the experimental results of this paper, the beam divergence varied between 0.1° and 0.03°. The beam spot was usually around 0.3 mm^2.

The crystals were mounted in a goniometer with a 360° rotation axis Φ and two perpendicular axes ψ and θ. The goniometer angle reading is accurate to within 0.01°. The goniometer is equipped with a cooling system by means of which the target temperature can be lowered to 100 °K. The arrangement of the detectors was the same as that described in Ref. 16. In the latest experiments, the Rutherford scattering detector B was replaced by an annular solid-state detector, covering scattering angles from 5° to 10°. For thicker crystals, this detector was moved to larger angles in order to avoid multiple scattering. The beam current was measured with a rotating scintillation system, which remained in the beam during 25% of the running time.

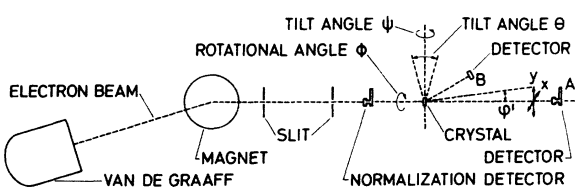

FIG. 1. Schematic drawing of the experimental setup.

III. CRYSTAL PREPARATION

The growth and test techniques of the thin silver and gold crystals were the same as those described in Ref. 16. The Au crystals were grown on mica, whereas the Ag crystals were grown on NaCl crystals pre-irradiated with x rays in order to create good nucleation centers. The thin Si crystals were fabricated by means of an etching technique as described by Meek *et al.*[18] The crystals turned out to be very good, giving dips in Rutherford scattering yield of protons down to ~ 2% of normal yield for the Si crystals and down to ~ 4% for the Ag and Au crystals.

By tilting and rotating the crystals and measuring the number of electrons transmitted in the forward direction, the orientation of the sample could be obtained. For a thin crystal, the variation in transmission yield, from which the alignment is obtained, is seen in Fig. 2(a). For the thicker crystals, the distribution of the transmitted electrons around a planar direction is quite different [Fig. 2(b)]. It is observed that whenever the angle between the beam and the plane is close to a Bragg position, an anomalous transmission yield is obtained. This effect was used to align the thicker crystals.

IV. RESULTS

Mainly two sets of experiments have been performed: namely, wide-angle Rutherford scattering as a function of the angle between the beam direction and either an axial or a planar direction (the yields are normalized to the average yield in a random direction); transmission experiments, where the angular distribution of electrons transmitted around the forward direction is measured.

A. Rutherford Scattering

Figure 3 shows the Rutherford scattering yield of 1.5-MeV electrons incident on a [100] axis [Fig. 3(a)] and a (110) plane [Fig. 3(b)] of a 2400-Å-thick Si crystal. In the axial case, the yield displays a peak of up to three times normal yield. The small "humps" at $\theta = \pm 0.6°$ are presumably

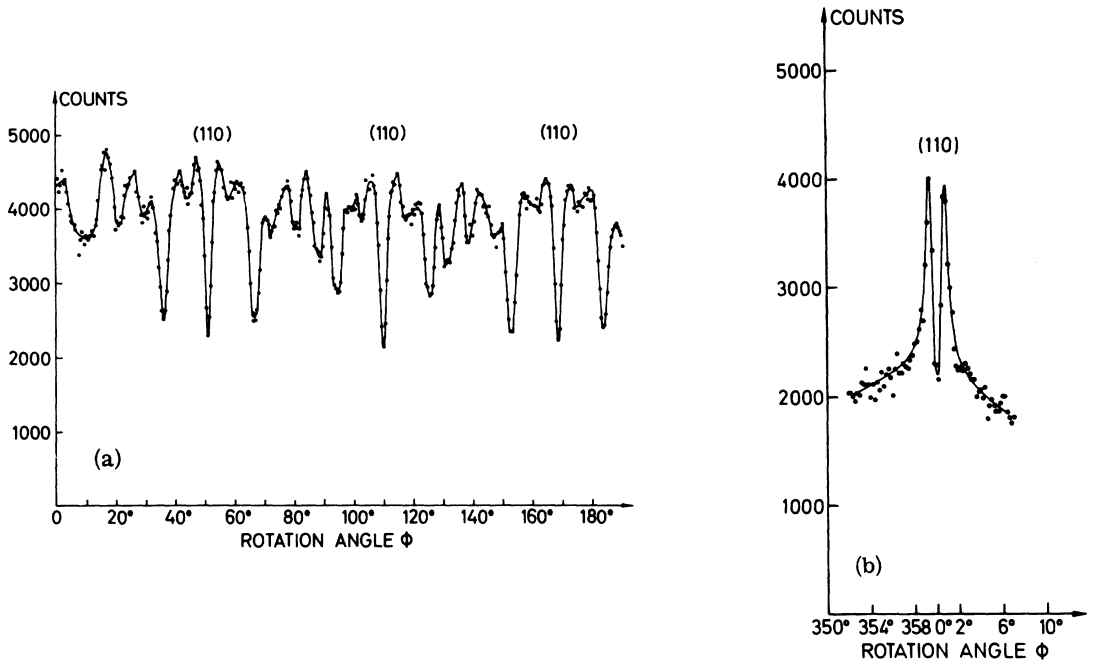

FIG. 2. Orientation dependence of the electrons transmitted in the forward direction. (a) Scan is a rotation around the [111] axis with the tilt angle θ held at 15°. Electron energy: 1 MeV. Foil was a 300-Å-thick Au crystal. (b) A small section of the total 360° rotation scan across a (110) plane. Electron energy: 1.5 MeV. Thickness of Si crystal: ~6 μm.

due to planar effects, as it is very difficult to tilt through a crystal axis without getting some influence on the scattering yield from the planes. Figure 3(b) shows that also planes give rise to a very pronounced peak in yield when the beam is aligned with a major planar direction. In the present case, the rise in yield is about 70% of normal yield.

In order to estimate the influence of planar effects on measurements of axial Rutherford scattering peaks, detailed parallel scans in the neighborhood of the [100] direction in the 2400-Å-thick Si crystal were made. Also here, the electron energy was 1.5 MeV. Figure 4 shows the intensity contours around the axis. It is seen that the low-index planes show very pronounced effects: even a number of minor planes may be identified; it is therefore rather difficult to find a "random" direction. Hence the choice of "normal scattering yield" is somewhat arbitrary which, in turn, introduces some uncertainty in the determination of the full width at half-maximum (FWHM) $\Delta\psi$ of the peaks.

In order to study the compensation effect of the negative shoulders for the planes, the yield $P(\theta, \psi)$ in the contour curves has been integrated along the azimuthal angle ϑ for a fixed distance φ from the [100] axis, i.e.,

$$I(\varphi) = (2\pi\varphi)^{-1} \int_0^{2\pi} P(\theta, \psi) d\vartheta;$$

$$\theta^2 + \psi^2 = \varphi^2; \quad \cos\vartheta = \theta/\varphi.$$

$I(\varphi)$ is shown in Fig. 5. A comparison of the FWHM $\Delta\psi_I$ of $I(\varphi)$ with $\Delta\psi$ values from different single scans though the [100] axis [see, e.g., Fig. 3(a)], shows that the $\Delta\psi$ values vary at most 10-15% from $\Delta\psi_I$. From $I(\varphi)$ is also seen that the compensation for the planes is almost complete. Furthermore, the negative compensation for this axis is rather shallow and stretches far out (~ 3°). The peak height of $I(\varphi)$ is seen to be a little lower than shown in Fig. 3. This may be due to the above-mentioned uncertainty in random level for scans through axial directions, and as the variation in peak height is small, the peak height is a rather well-defined experimental parameter.

Figure 6 shows the Rutherford scattering yield for 1.5-MeV electrons incident on Si crystals of different thicknesses. The scans are obtained for either the [100] (a, c) or the [110] (b, d) direction. It is noted that the peak height decreases strongly with increasing thickness, whereas the critical angle $\Delta\psi$, defined as the FWHM, increases, if at all, very slowly. The same tendency was found in the gold experiments (Fig. 7 of Ref. 16).

Figures 7 and 8 show the Rutherford scattering

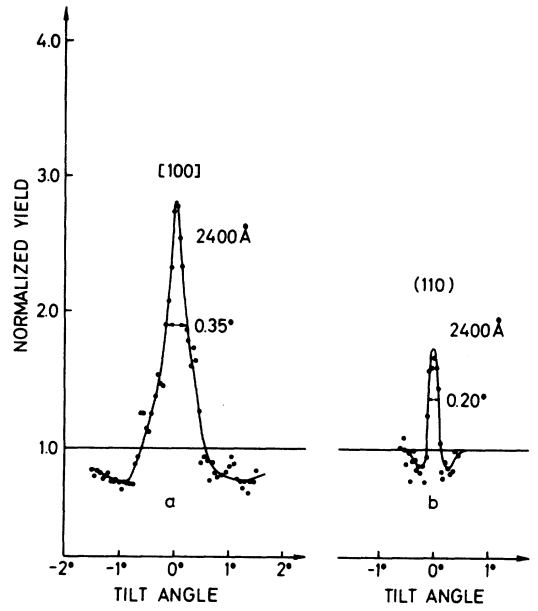

FIG. 3. Normalized Rutherford scattering yield of 1.5-MeV electrons incident on a 2400-Å-thick Si crystal. (a) [100] axis, (b) (110) plane.

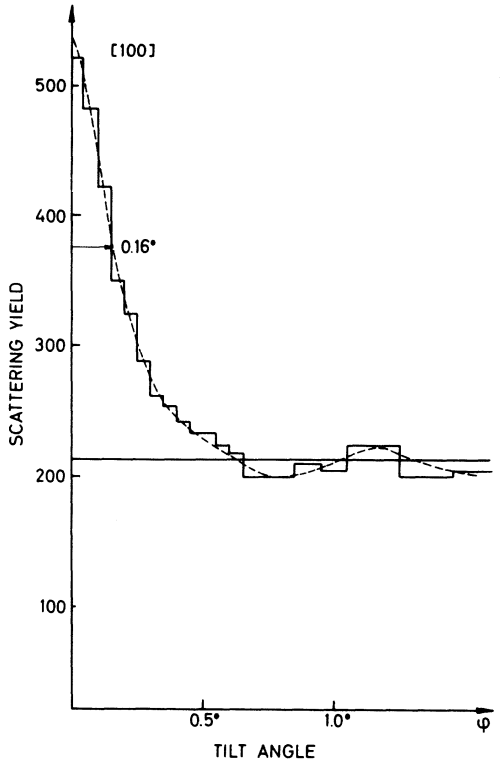

FIG. 5. The $P(\theta, \psi)$ yield in the contour plot from Fig. 4 integrated along the azimuthal angle ϑ for a fixed distance φ from the [100] axis. The dashed curve is smoothly drawn through the histogram obtained by the numerical integration of $P(\theta, \psi)$. For $\varphi \leq 0.05°$, the statistical uncertainty is 5–10%, whereas for $\varphi \geq 1°$, this uncertainty is < 0.5%.

yield from a 600- and a 1200-Å gold crystal (the [111] direction) as a function of energy. It is seen that the scan at 1.0 MeV is a little asymmetric and shows small peaks for negative tilt angles due to the fact that the scan was a little off center,

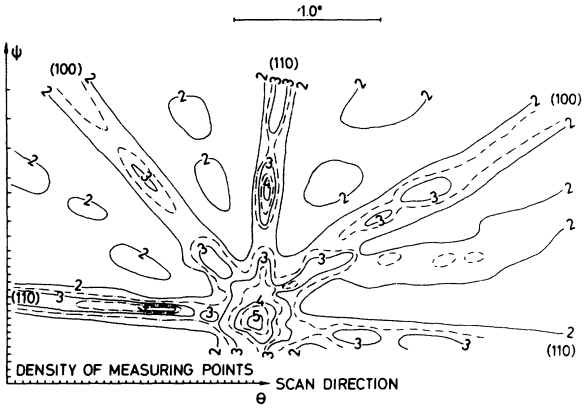

FIG. 4. Two-dimensional contour plot around the [100] axis of the Rutherford scattering yield of 1.5-MeV electrons incident on a 2400-Å Si crystal. Parallel scans were taken from fixed ψ values in the θ direction. The ψ axis indicates the number of scans taken, and the θ axis the distance between the measuring points in every scan. Numbers on solid lines represent counts in hundreds (100, 200, etc.). Dash-dot lines between solid lines represent 150, 250, etc. counts.

but as mentioned above, the variation in $\Delta\psi$ values are at most ~ 10%. The peak height is nearly independent of energy variations from 0.6 to 2.0 MeV, whereas the critical angle $\Delta\psi$ varies within experimental uncertainty as $(pv)^{-1/2}$, where p is the relativistic momentum and v is the velocity. For protons, the 1200-Å-thick Au crystal showed a Rutherford scattering yield of only ~ 4%, while the minimum yield for the 600-Å Au crystal was 10%.

B. Reversibility

An important concept in Lindhard's theoretical description[2] of directional effects is the rule of reversibility (reciprocity theorem[19]). This rule is observed to hold for heavy particles (see Refs. 20 and 21) and is often involved when measurements of the reaction yield as a function of angle of incidence are compared with calculations, since many of such calculations are directly concerned with the emission of particles from a lattice site. Figures 9 and 10 show an experimental demon-

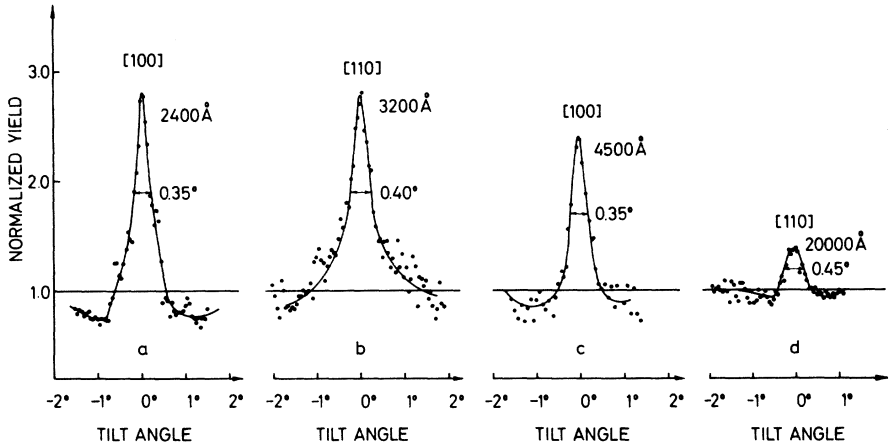

FIG. 6. Variation of the Rutherford scattering yield for 1.5-MeV electrons incident on Si crystals of different thicknesses. (a) [100] axis, 2400 Å; (b) [110] axis, 3200 Å; (c) [100] axis, 4500 Å; (d) [110] axis, 20 000 Å.

stration of the validity of the rule for electrons. The principle in the experimental setup is shown in Fig. 9. A 1.5-MeV electron beam is incident on a 1200-Å [111] Au crystal. Rutherford-scattered electrons are detected by a solid-state detector. By varying the angle φ between the incoming beam and the [111] axis and keeping the angle ψ constant, the Rutherford scattering yield may be measured as a function of the angle of incidence. The emission case is simulated by measuring the scattering yield for varying ψ and fixed φ. Here φ must be a large angle in order to simulate emission from the nuclei.

The results of such experiments are shown in Fig. 10. The abscissa is the angle relative to the [111] direction, i.e., in the "incoming-beam" case, the angle φ and in the "outgoing-beam" case the angle $\psi - \varphi$. Both curves are normalized to the average yield in random direction. The two curves have the same FWHM $\Delta\psi$ and peak heights, and hence the rule of reversibility is well justified.

C. Transmission Experiment

Intensity measurements in the forward direction have mainly been made in order to orient the crystal as described in Sec. III. If the zero-order Bragg-beam intensity $|\psi_{\vec{g}=0}|$ (here $\vec{g}$ is the reciprocal-lattice vector) is measured as a function of φ, pronounced and sharp dips are obtained. This is partly due to the fact that if φ tends to zero, strong elastic Bragg beams are excited, and partly to the fact that at the same time, the inelastic (thermal-diffuse) background is increased (increased absorption at the symmetry position). Photographs of the transmitted intensity show that in the symmetry position for, e.g., [110] Si at 1.5 MeV, up to 60 Bragg beams are visible. In order to show the increase in inelastic scattering for the [111] direction of a 1200-Å Au foil at 1 MeV, a two-dimensional intensity scan in the forward direction was made for every fixed φ, and the total elastic intensity $\sum_{\vec{g}} |\psi_{\vec{g}}|^2$ in the Bragg spots summed up. Indeed, as $\varphi \to 0$, the elastic intensity drops on account of inelastic scattering. The experimental uncertainty does not allow an unambiguous determination of the FWHM, but at least it seems not to be far off $\Delta\psi_{[111]}$.

The main purpose of this work has been to show that in the limit of large quantum numbers, electron channeling can be approximately described by a classical model (see Sec. V). Therefore mainly atomic strings have been investigated since there the potential hole is much stronger than for planes. Nevertheless, some planar effects have also been studied. Figure 11 shows the variation in Rutherford scattering yield around the (100) and (110) planes. The electron energy was 1.5 MeV,

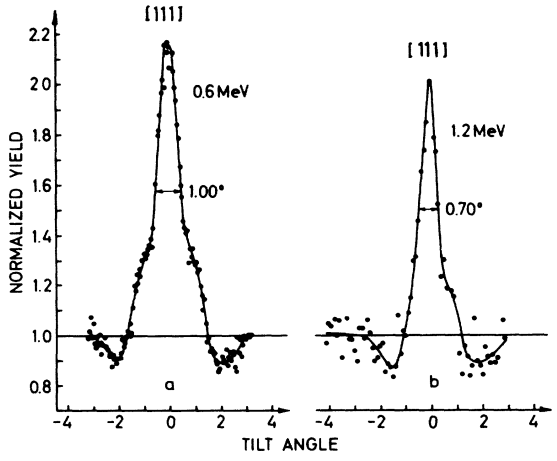

FIG. 7. Energy variation of Rutherford scattering yield for electrons incident on a ~600-Å-thick Au crystal.

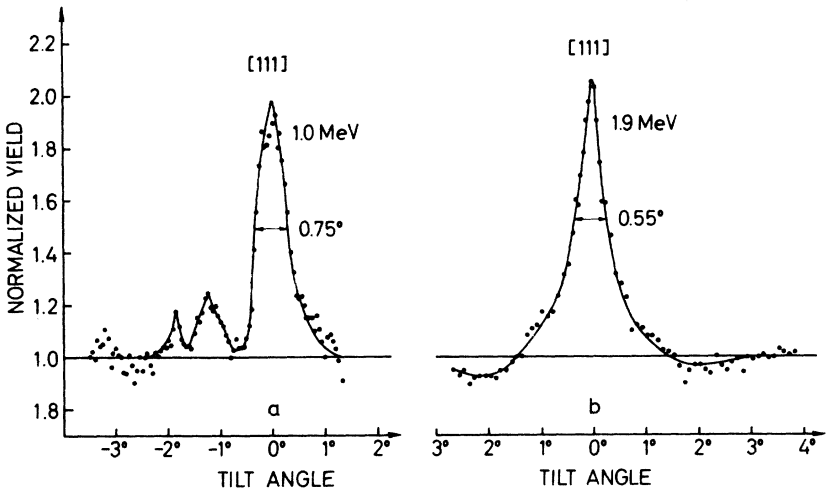

FIG. 8. Energy variation of Rutherford scattering yield for electrons incident on a ~1200-Å-thick Au crystal.

and the crystal thickness varied from 2400 to 20 000 Å. Also for planes, the $\Delta\psi$ values are almost independent of crystal thickness, and the peak decreases rather rapidly. The negative compensation for a planar peak occurs at angles immediately outside the peak region.

Film exposures have been made in order to study the connection between the channeling effect in Rutherford scattering, obtained in thin crystals, and the Kikuchi defect bands, normally obtained in the forward direction for thick crystals. Figure 12(a) shows excess bands in the Rutherford scattering region for a 3200-Å Si crystal at 1.5 MeV. The intensity in the forward direction is roughly five orders of magnitude higher than that found where the bands are observed. Hence no Bragg spots are visible since the film was overexposed in this region. According to the reciprocity theorem, these bands reflect the increase in Rutherford yield caused by channeling.

In contrast to this, Fig. 12(b) shows for a 6-μm Si crystal at 1.5 MeV a Kikuchi (220) defect band; the picture was taken with the electron beam aligned with the plane (the "systematic" case of electron diffraction). In addition to the photographs, scans of the intensity distribution across the bands under discussion have been made by means of the solid-state detectors: Figure 13(a) shows the Rutherford yield, Fig. 13(b) the zero-order Bragg intensity $|\psi_{\vec{g}=0}|^2$, and Fig. 13(c) the Kikuchi-band intensity distribution. Figures 13(a) and 13(b) are obtained by varying the angle of incidence φ in the thin crystal; Fig. 13(c) by changing the scattering angle φ' in the forward direction. It turns out that the intensity distributions in Figs. 13(a) and 13(c) are opposite to one another and that the "critical" angles are nearly identical. The $|\psi_{\vec{g}=0}|^2$ distribution is roughly that of the Kikuchi band, despite the fact that the FWHM is larger.

V. DISCUSSION

The discussion will mainly follow two lines.

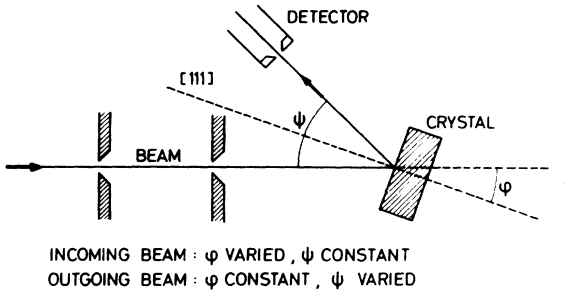

FIG. 9. Illustration of the principles in the reversibility experiment.

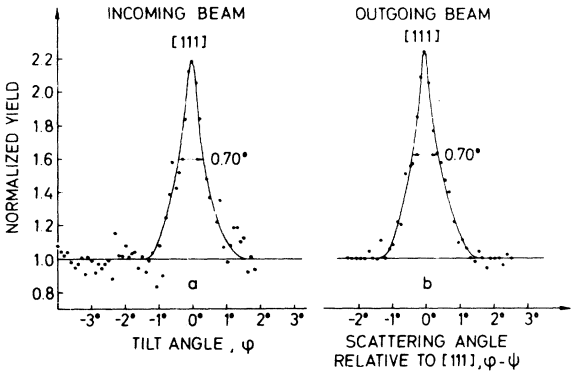

FIG. 10. Results of the reversibility experiment. In (a) the angle ψ was around 30° and in (b) both ψ and φ were around 30°.

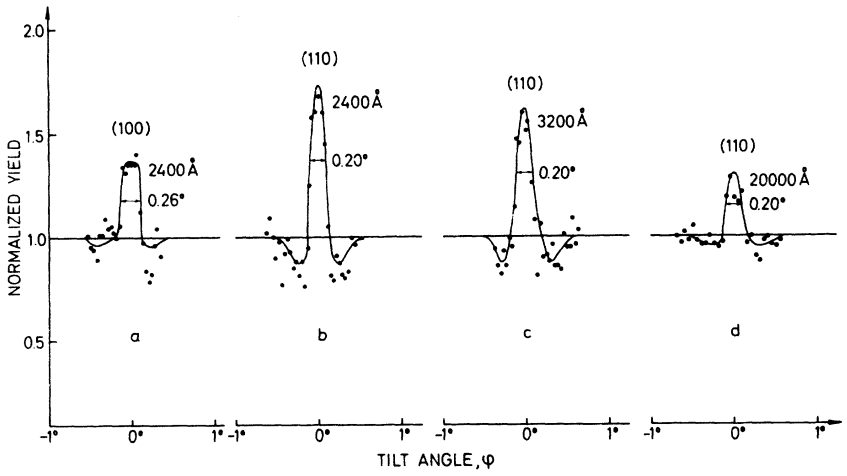

FIG. 11. Normalized Rutherford scattering yield of 1.5-MeV electrons incident on Si crystals. (a) (100) plane, 2400 Å; (b) (110) plane, 2400 Å; (c) (110) plane, 3200 Å; (d) (110) plane, 20 000 Å.

In Sec. V A the results are discussed on the basis of a wave-mechanical treatment. For this, a rather extensive study of the n-beam treatment of the dynamical theory of diffraction has been made. Sec. V B will then deal with the question of the extent to which a classical channeling theory can approximately describe the experiments.

A. Many-Beam Calculations of the Backscattering Yield

The dynamical theory of electron diffraction has been discussed by many authors (see, e.g., Ref. 13). The basic set of equations for this theory is given by a Bloch-wave solution of the Klein-Gordon equation in a three-dimensional periodic potential. By using the projection approximation,[12] which yields a Schrödinger equation for the transverse motion where the kinetic-energy operator contains the relativistic mass, it is possible to Fourier expand the Bloch waves and the potential in the reciprocal lattice on a plane (for an axis in real space; cross-grating pattern) or a line (for a plane in real space; systematic reflection) that is perpendicular to the axial or planar direction. If only a finite number of points has to be considered, the solution of the basic equation can be transformed into a standard eigenvalue problem. By matching the wave function inside the crystal to the incoming plane wave, the amplitude C_0^i and the plane-wave coefficient $C_{\vec{g}}^i$ in the ith Bloch wave are obtained. The Fourier components of the crystal potential $V(\vec{r})$ in the present calculations are taken from Doyle and Turner.[22] Absorption effects are treated as a perturbation and taken into account by adding a periodic imaginary potential $iV'(\vec{r})$ to the crystal potential $V(\vec{r})$. In the present calculations, a linear approximation to the Humphreys and Hirsch[23] values of $V'_{\vec{g}}/V_{\vec{g}}$ for single-electron and phonon scattering has been used. The absorption strength used here is the same as that used for transmission, but the results indicate that the absorption for Rutherford scattering, especially for gold, is somewhat different. The Rutherford scat-

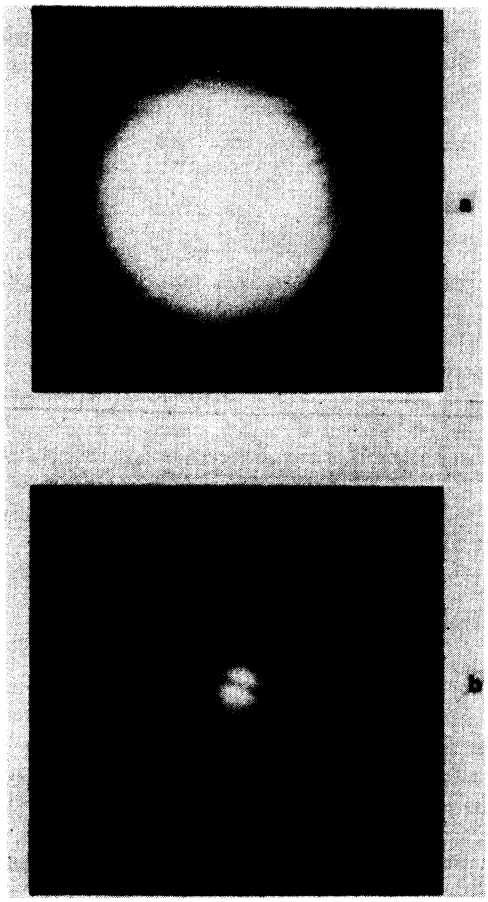

FIG. 12. (a) Photograph showing excess bands in the Rutherford scattering region for a 3200-Å-thick Si crystal. The electron energy was 1.5 MeV; (b) photograph showing a (220) Kikuchi defect band for a 6-μm-thick Si crystal. Electron energy: 1.5 MeV.

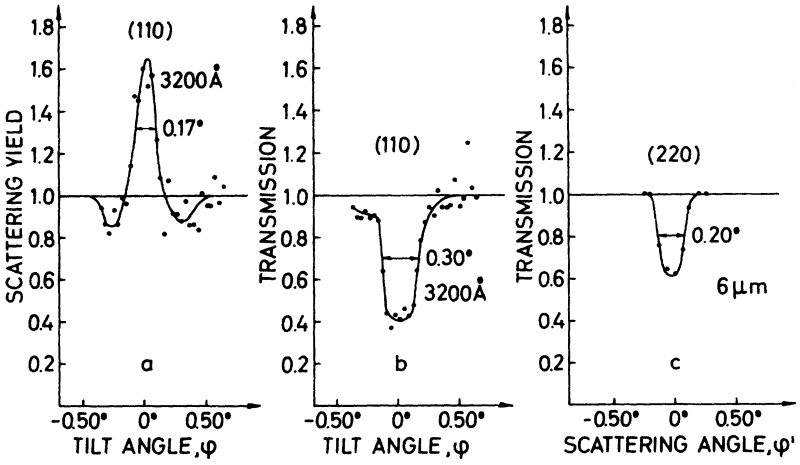

FIG. 13. (a) Rutherford scattering yield of 1.5-MeV electrons incident on a 3200-Å-thick Si crystal as a function of beam direction relative to the (110) plane; (b) zero-order Bragg-beam intensity obtained under the same conditions as in (a); (c) scan with the transmission detector across the (220) Kikuchi defect band shown in Fig. 12(b). Both (b) and (c) show the normalized transmission yield.

tering yield without absorption $I_R(\varphi)$ is assumed to be proportional to the incoherently added Bloch-wave intensity at the atomic positions. These positions have been distributed as a Gaussian, which accounts for the thermally vibrating atoms. Thus the Rutherford scattering probability I^i for the Bloch wave i is obtained:

$$I^i = I_0 \sum_{\vec{g},\vec{g}'} C^i_{\vec{g}} C^{i*}_{\vec{g}'} D_{\vec{g}-\vec{g}'}, \tag{1}$$

with

$$D_{\vec{g}} = e^{-M_{\vec{g}}}; \quad M_{\vec{g}} = \tfrac{2}{3}\pi^2(\vec{g})^2\rho^2,$$

where ρ^2 is the mean-square thermal amplitude (i.e., the three-dimensional one) and I_0 is a normalizing constant. The total Rutherford scattering intensity is then given by

$$I_R(\varphi) = \sum_i |C^i_0|^2 I^i. \tag{2}$$

When absorption is taken into account, it has been assumed that electrons removed from Bloch wave i due to inelastic scattering behave as plane waves. Hence the Rutherford scattering intensity with absorption can be written as

$$I_R(\varphi, t) = \sum_i |C^i_0|^2 I^i \int_0^t e^{-4\pi q^i z} dz + I_0 \int_0^t \left(1 - \sum_i |C^i_0|^2 e^{-4\pi q^i z}\right) dz.$$

The first term gives the intensity from the attenuated Bloch waves integrated over thickness, and the second term gives the intensity from the plane wave integrated over thickness.

The smearing effect of the thermal vibrations can also be taken into account by multiplying the Fourier components of the crystal potential by Debye-Waller factors D_g. The convergence of the calculations was investigated by increasing the number of beams.[24]

1. String Case

Figure 14(c) shows the theoretical curves $I_R(\varphi, t)$ for 1.5-MeV electrons incident along the [100] axis in 2400-Å Si. The theoretical curves have been folded with the beam profile, which has an angular opening of 0.03°. It is seen that at 91 beams, the convergence is still not satisfactory. In Fig. 14(a) is shown a comparison between the 91-beam calculation and experimental results. As far as the peak height and the FWHM $\Delta\psi$ are concerned, the agreement is good. Because of the lack of convergence, the calculated peak should be even more pronounced. A comparison between calculated [$I_R(\varphi)$, 91 beams] and experimental results for 1-MeV electrons on a [110] axis in Au is shown in Fig. 14(b). The agreement is not quite as good as that in the Si case; this may be due to the fact that the number of beams is much too low.

In Ref. 14, the number of beams to be used is discussed, and it is pointed out that a good estimate for the number of beams n is $4(\Delta\psi/\psi_B)^2$ and $2(\Delta\psi/\psi_B)$ for the axial and planar case, respectively, ψ_B is the corresponding Bragg angle.

As shown below, the observed width of the channeling peak for the axis is very close to $0.7\,\psi_1$, where ψ_1 is Lindhard's critical angle; e.g.,

$$4(\Delta\psi/\psi_B)^2 \approx 2(\psi_1/\psi_B)^2 = \frac{8 d_s^2 Z_2 m}{d a_0 \pi^2 m_0},$$

where d_s is the distance between the strings in the lattice, Z_2 is the atomic number of the target atom, a_0 is the Bohr radius, d is the spacing of atoms in a string, and m/m_0 is the ratio between the relativistic mass and the rest mass of the electron, respectively. For the [100] Si case, $n \approx 115$, whereas in the case of 1-MeV electrons on a [110] gold axis, $n \approx 1000$. Hence in the gold case, the calculations cannot be expected to give a good fit.

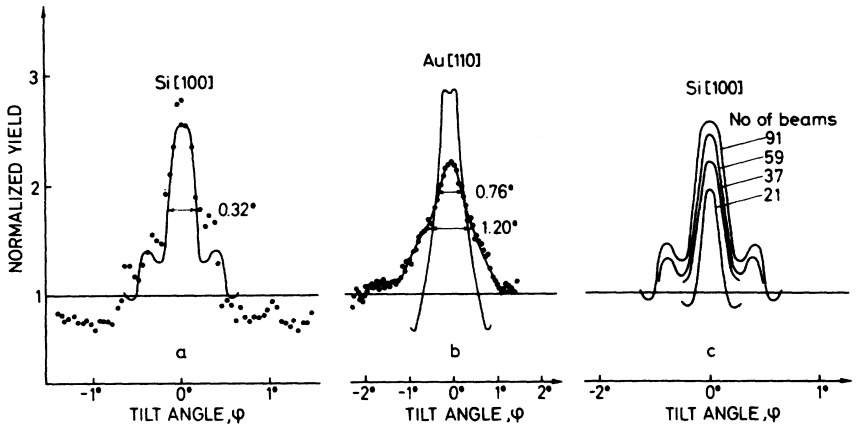

FIG. 14. (a) Comparison between a 91-beam calculation and the experimental Rutherford scattering yield for 1.5-MeV electrons incident on a 2400-Å-thick Si crystal in the [100] direction. (b) Comparison between a 91-beam calculation and the experimental Rutherford scattering yield for 1-MeV electrons incident on a 1500-Å-thick Au crystal in the [110] direction. (c) Many-beam calculation of the Rutherford scattering yield for 1.5-MeV electrons incident along the [100] axis in a 2400-Å-thick Si crystal.

Besides, the strength of the absorption is questionable.

2. *Planar Case*

Figure 15 shows a comparison between the calculated curves [20-beam calculations, $I_R(\varphi, t)$ convoluted with the beam divergence] and experimental curves for 1.5-MeV electrons incident along the (100) and (110) planes in Si. The agreement is good. It is also seen that the variation in the half-widths is almost inversely proportional to the distance d_p between the lattice planes, whereas in a classical description the critical planar angles are directly proportional to the square root of the planar distance.

Figure 16 shows a comparison between the experimental curves of Fig. 13 and the theoretical ones for the (110) plane in Si at 1.5 MeV. The calculated Rutherford scattering yield and the zero-order intensity $|\psi_{\vec{g}=0}|^2$ have been obtained for 3200 Å, while the added Bragg-beam intensity $\sum_{\vec{g}}|\psi_{\vec{g}}|^2$ was obtained for 6 μm. According to the Kikuchi-band theory of Thomas and Humphreys,[25] the total Bragg-beam intensity as a function of the incident angle φ should be equal to the Kikuchi-band profile $I_K(\varphi')$. Figure 16 shows that this is actually so. Furthermore, since $\sum_{\vec{g}}|\psi_{\vec{g}}|^2$ is equal to the Bloch-wave intensity at the exit surface of the crystal,

$$\sum_{\vec{g}} |\psi_{\vec{g}}|^2 = I_K(\varphi') = \sum_i |C_0^i|^2 e^{-4\pi q^i z}, \tag{3}$$

where q^i is the absorption coefficient. Thus, for not too thick crystals,

$$I_K(\varphi') \approx 1 - 4\pi z \sum_i |C_0^i|^2 q^i = 1 - \frac{4\pi m z}{\hbar^2 K} \sum_i |C_0^i|^2 \sum_{\vec{g},\vec{g}'} C_{\vec{g}}^i C_{\vec{g}'}^{i*} V'_{\vec{g}-\vec{g}'}. \tag{4}$$

Here, m is the electron mass, K is the wave vector outside the crystal, and $V'_{\vec{g}}$ is the Fourier component of the imaginary potential. Looking at the Fourier components of $V'_{\vec{g}}$, it seems to be a rather good approximation, at least for orders that are not too high, to set

$$V'_{\vec{g}} \propto D_{\vec{g}}.$$

Thus, together with Eqs. (1) and (2), we find

$$I_K(\varphi') \approx 1 - \alpha I_R(\varphi), \tag{5}$$

where α is a constant, independent of angle. Hence, for crystals which are not too thick, the Kikuchi-band profile [Fig. 16(c)] in the forward direction should be just the opposite of the Rutherford-yield curve of Fig. 16(a) or, equivalently, the bands in Fig. 12(a) wide-angle Kikuchi bands. While the derivation of Eq. (5) holds for rather thin crystals only, it has been shown by Thomas *et al.*[25] that

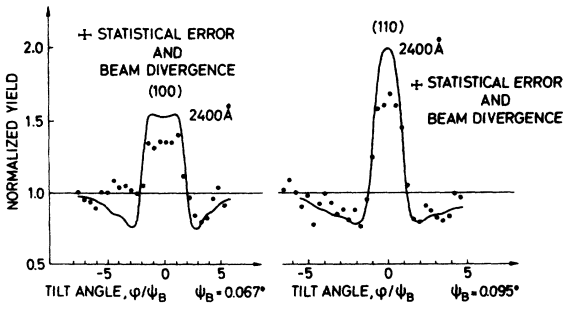

FIG. 15. Comparison between many-beam calculation and experimental Rutherford scattering yield for 1.5-MeV electrons along the (100) and (110) planes in a 2400-Å-thick Si crystal. ψ_B is the Bragg angle. The number of beams in the calculations was 20.

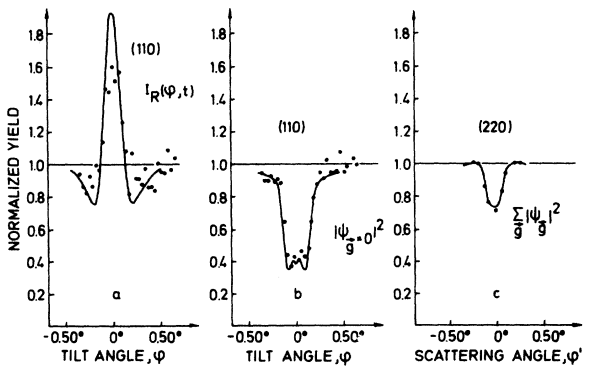

FIG. 16. Comparison of the experimental curves of Fig. 13 and many-beam calculations (20-beam calculation).

the angular shape of the Kikuchi bands, $I_K(\varphi')$, in the forward direction is rather insensitive to foil thickness. Wide-angle Kikuchi bands at low energies have been investigated experimentally by Alain *et al.*[26]

B. Classical Description

In Ref. 7, Lindhard discusses the circumstances under which electron channeling can be described by classical mechanics. As one of the conditions for the applicability of a classical description, he requires that the number ν of bound states in the string or planar potential holes be large compared to unity. For strings,

$$\nu_s=\frac{1}{h^2}\iint d^2r\,d^2p_\perp>1;\quad E_\perp\leq 0, \tag{6}$$

where $E_\perp=p_\perp^2/(2m)+U(r)$, $p_\perp$ being the transverse momentum and m the relativistic mass.

From Lindhard's standard potential $U(r)=(Z_1Z_2e^2/d)\ln[(Ca/r)^2+1]$ for strings and with $Z_1=-1$, it is found that

$$\nu_s=\frac{1}{(1-v^2/c^2)^{1/2}}\,Z_2^{1/3}\,\frac{4a_0}{d}\ . \tag{7}$$

By applying the corresponding planar potential, we arrive at the following formula for the case of planes:

$$\nu_p=\frac{1}{h}\iint dy\,dp_\perp\simeq\frac{4a_0(Nd_p)^{1/2}}{(1-v^2/c^2)^{1/4}}\ . \tag{8}$$

Here v and c are the velocities of the electron and light, respectively, N is the density of the target atoms, and d_p is the planar spacing.

In our case, the ν_s values range from ~3 to 10, which shows that for almost all of our string results, it is reasonable to compare with classical calculations, whereas the ν_p values are $\lesssim 2$; hence the planar effects cannot be expected to be accounted for classically.

Naturally, interference effects are expected because of the periodic position of the strings in the lattice. As was found above, the ratio between the Bragg angle and Lindhard's critical angle is usually small compared to unity, and thus interference effects are expected to appear only as fine-structure patterns in the string effect.

1. String Case

Because of the rule of reversibility (reciprocity), which was shown above to hold also for electrons, the distribution in the Rutherford scattering yield from an external beam is identical to the distribution of electrons emitted from lattice sites; hence considerations that hold for Rutherford scattering can be applied to the emission picture and vice versa. In Lindhard's paper,[7] the yield $I_R(\varphi)$ consists of the peak yield I_R^P for angles $\varphi\lesssim\psi_1$ and a negative shallow compensation I_R^C stretching out to angles φ somewhat larger than Ca/d. This means that the integral of I_R over the entire solid angle is zero. It can be shown that for angles $\varphi\sim Ca/d$, 30% of the peak is still not compensated for. For $I_R^P(\varphi)$ it is found that

$$I_R^P(\varphi)\simeq e^{-2\varphi^2/\psi_1^2}\ln\alpha\gamma,\quad \alpha\gg 1 \tag{9}$$

where ψ_1 is the critical angle, $\gamma=1.78$, the Euler constant, $\alpha=C^2a^2/\rho^2$ with $C^2\approx 3$, a the Thomas-Fermi screening distance, and ρ^2 the mean-square thermal vibrational amplitude in two dimensions. From this expression for the FWHM, $\Delta\psi$ is found to be

$$\Delta\psi=(2\ln 2)^{1/2}\psi_1\approx 1.2\psi_1 \tag{10}$$

and the peak height $I_R^P(0)=\ln(\alpha\gamma)$.

In the calculation of the above expression for the excess yield $I_R^P(\varphi)$ it is assumed that multiple scattering can be disregarded. Although it is by no means a simple matter to obtain $I_R^P(\varphi,t)$ as a function of thickness (partly because of lack of information about scattering cross sections and partly because of difficulties in calculation), the integral

$$\omega=\int I_R^P(\varphi)\,2\pi\varphi\,d\varphi=\tfrac{1}{2}\pi\psi_1^2\ln(\alpha\gamma),\quad \alpha\gg 1 \tag{11}$$

should remain approximately constant until the depth where the multiple scattering width Ω is comparable to a/d.[16]

Lindhard[7] obtained the rather simple formula for $I_R^P(\varphi)$ by using a cutoff in the standard potential. From this potential, but without such a cutoff, Andersen *et al.*[15] arrived at an analytical expression for the distribution, viz.,

$$\hat{I}_R^P(\varphi)=e^{-2\varphi^2/\psi_1^2}\times\ln\left(\frac{1+C^2a^2\gamma/e\rho^2-e^{-2\varphi^2/\psi_1^2}}{1+(Ca/r_0)^2-e^{-2\varphi^2/\psi_1^2}}\right). \tag{12}$$

The two distributions have the common feature that the FWHM $\Delta\psi$ is proportional to Lindhard's critical angle ψ_1 because the standard potential introduces a scaling of transverse energy with $E\psi_1^2$.

In the Rutherford scattering experiments shown in the present paper, the energy loss of the electrons is much smaller than the energy resolution of the detector system. Hence all of the measured Rutherford scattering distributions represent an average channeling effect for electrons penetrating to all possible depths in the crystal before being scattered. The experimental distribution from the very thin Si crystal (Fig. 3) might be close to the distribution from a crystal thin enough for multiple scattering to be neglected. The distribution $\hat{I}_R^P(\varphi)$ in formula (12) has been folded with a normal Gaussian multiple scattering distribution (see Fig. 17). The scattering is, of course, underestimated as multiple scattering is much more pronounced in the axial than in the random direction. It is seen that because of multiple scattering, the electrons in the peak are scattered very rapidly to wider angles, thus giving rise to an increased yield at these angles. However, the rise is of the order of a few percent only, and for the distributions integrated over depths, the FWHM stays nearly constant as a function of crystal thickness. This is seen to hold for both the gold and the silicon cases shown in Fig. 6. This, in turn,

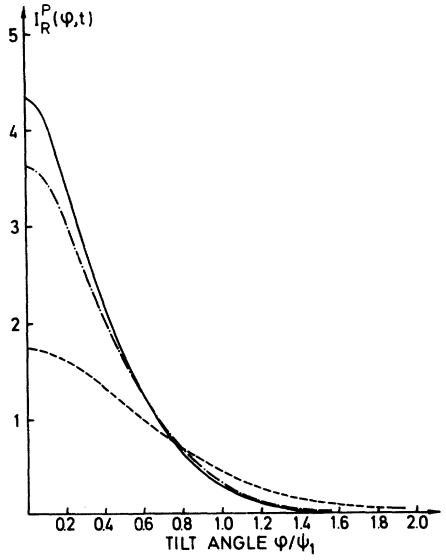

FIG. 17. $\hat{f}_R^P(\varphi,t)$ convoluted with a Gaussian multiple scattering distribution and integrated over crystal thickness. Full line: distribution without multiple scattering for 1.5-MeV electrons incident along the [100] axis; dot-dash line: the same distribution convoluted with a Gaussian and integrated over ~2000 Å; and broken line: integrated over ~1.6 μm.

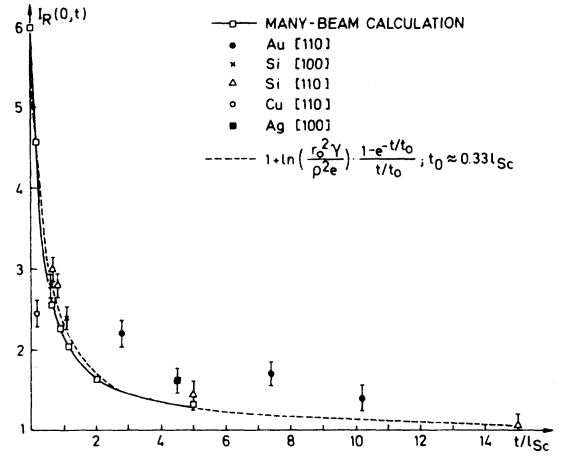

FIG. 18. Experimental peak heights $I_R(0,t)$ plotted as functions of t/l_{sc}, where t is the crystal thickness and l_{sc} the mean-free-path length for electrons in an amorphous substance.

means that the FWHM $\Delta\psi$ for all the present Rutherford scattering results can be compared with theoretical calculations. The decrease in peak height as a function of crystal thickness is shown in Fig. 18. Here, all the experimental peak heights are plotted as a function of the normalized thickness t/l_{sc}, where l_{sc} is the amorphous foil thickness corresponding to one scattering event[27]; i.e., $l_{sc}=(N\sigma)^{-1}$, where σ is the total cross section and N is the density of atoms in the foil. The dashed curve in Fig. 18 starts as an exponential and then changes into a linear dependence. It is seen that the Si data follow this curve within experimental error. The gold data do not fit the curve but have the same slope; this may be due to the low Debye temperature for gold, giving rise to a large thermal vibrational amplitude at room temperature ($\rho^2\sim 0.023$ Å^2). Preliminary experiments have shown a decrease in the $\Delta\psi$ value of around 25% for the [110] in gold when the target was cooled from room temperature to 100 °K. In the same plot is seen the thickness dependence of peak heights obtained from many-beam calculations. In the same plot are shown Cu data taken from Ref. 4. As shown above, the rule of reversibility holds for electrons, so the emission data in Ref. 4 can be compared with Rutherford scattering data. The copper results are seen to be much lower; however, this is to be expected since the crystal was damaged and thus showed a minimum yield in proton Rutherford scattering of 20%. For a perfect crystal, this yield should be ~3%.

In Table I, the experimental results are summarized. From the Au and Si data it is seen that

TABLE I. Comparison between d, ψ_1, $\Delta\psi$, $\Delta\psi/\psi_1$, and ν_s for different energies, axes, and crystals.

Crystal	E (MeV)	Axis	String constant d(Å)	ψ_1(deg)	FWHM $\Delta\psi$ (deg)	$\Delta\psi/\psi_1$	ν_s
Au	0.6	[111]	6.9	1.56	1.00 ± 0.05	0.64	3
	1.0	[110]	2.8	1.97	1.20 ± 0.05	0.61	9
		[111]	4.9	1.26	0.85 ± 0.05	0.67	5
		[112]	6.9	1.11	0.75 ± 0.05	0.67	4
	1.5	[111]	6.9	1.06	0.70 ± 0.05	0.66	5
	2.0	[111]	6.9	0.94	0.55 ± 0.03	0.59	6
Si	0.7	[110]	3.8	0.84	0.58 ± 0.05	0.69	3
		[111]	4.5	0.75	0.40 ± 0.05	0.53	2.5
	1.5	[100]	5.4	0.51	0.35 ± 0.03	0.69	4
		[110]	3.8	0.61	0.40 ± 0.03	0.66	5
	3.0	[100]	5.4	0.38	0.23 ± 0.03	0.61	6
Ag	1.5	[100]	4.07	1.08	0.80 ± 0.03	0.72	7
Cu	0.4	[110]	2.5	1.82	1.5 ± 0.4	0.80	4

the $\Delta\psi$ values are proportional to ψ_1 for a variation in string constant d and energy, ranging from 2.8 to 7 Å and from 0.6 to 3.0 MeV, respectively. The d dependence is not so nicely fulfilled for the 700-keV Si data, but the number of bound states ν_s is small. From the table it can also be seen that the Z_2 dependence of the $\Delta\psi$ values follows that of ψ_1, and the over-all factor of proportionality between $\Delta\psi$ and ψ_1 is approximately 0.7. Even then the copper data are only a little off, which is to be expected because of the damage. The question of the conservation of the peak volume for different depths in the crystal was discussed in Ref. 16, but in general, this is not so simple to investigate by means of Rutherford scattering because of the difficulties in connection with the definition of the random level. This effect can be studied in a better way by measuring the distribution of electrons emitted in a well-defined depth in a crystal and then changing the emission depth by etching down the crystal.

2. *Planar Case*

As shown above, the number of quantum states in phase space for planes is less than two. This means that the experimental results should not be compared with classical calculations. In Table II the experimental results for planes are summarrized. It is seen that, in general, the $\Delta\psi$ values are not proportional to ψ_p, the classical planar critical angle

$$\psi_p=\left(\frac{2Z_1Z_2e^2Nd_pCa}{\frac{1}{2}pv}\right)^{1/2}. \tag{15}$$

Here d_p is the distance between the planes. It is seen that ψ_p is proportional to $d_p^{1/2}$, which is not the case for the experimental $\Delta\psi$ values.

As shown (e.g., Fig. 15), the many-beam calculations, which for planes are comparatively simple, describe the experimental results rather well.

VI. CONCLUSION

For electrons, experimental results for planes are in good agreement with quantal calculations based upon the many-beam theory, but for the string case, the conventional wave theory, based upon plane-wave expansion, is rather time consuming since the number of waves required is large ($\gtrsim 100$). For the string case, the experimental results are found to be in good agreement with classical calculations whenever the number of

TABLE II. Comparison between d_p, ψ_p, $\Delta\psi$, FWHM for many-beam calculation and ν_p for different energies, planes, and crystals.

Crystal	E (MeV)	Plane	Planar constant d_p (Å)	ψ_p (deg)	FWHM $\Delta\psi$ (deg)	FWHM Many beam (deg)	ν_p
Au	1	(110)	1.44	0.42	0.30 ± 0.03	0.35	1.8
	1.5	(110)	1.44	0.35	0.23 ± 0.03	0.25	2.4
Si	1.5	(110)	1.92	0.19	0.20 ± 0.03	0.18	1.3
	1.5	(100)	1.36	0.16	0.26 ± 0.03	0.27	1.1

bound states ν_s in phase space is rather large (Lindhard's criterion).

ACKNOWLEDGMENTS

The authors are indebted to J. U. Andersen, E. Bonderup, and J. Lindhard for fruitful discussions. We also want to thank A. Howie for supervising and very fruitful discussions in setting up the computer program for the many-beam calculations. It is a pleasure for one of us (F. B.) to thank R. Sizmann for encouraging stimulation. It is also a pleasure to thank R. L. Meek, Bell Telephone Laboratories, and P. Ambrosius-Olesen, who made the crystals.

---

*Permanent address: Sektion Physik der Universität München, Munich, Germany.

†Present address: Bell Telephone Laboratories, Mountain Ave., Murray Hill, N.J. 07974.

[1]S. Datz, C. Erginsoy, G. Liebfreid, and H. O. Lutz, Annu. Rev. Nucl. Sci. **17**, 129 (1967).

[2]J. Lindhard, K. Dan. Vidensk. Selsk. Mat.-Fys. Medd. 34, No. 14 (1965).

[3]P. Lervig, J. Lindhard, and V. Nielsen, Nucl. Phys. A. **96**, 481 (1967).

[4]E. Uggerhøj and J. U. Andersen, Can. J. Phys. **46**, 543 (1968).

[5]J. U. Andersen, W. M. Augustyniak, and E. Uggerhøj, Phys. Rev. B **3**, 705 (1971).

[6]M. J. Pedersen, J. U. Andersen, and W. M. Augustyniak, Radiat. Eff. **12**, 47 (1972).

[7]J. Lindhard, in *Atomic Collision Phenomena in Solids* (North-Holland, Amsterdam, 1970), p. 1.

[8]F. Bell, H. J. Kreiner, and R. Sizmann, Phys. Lett. A **38**, 373 (1972).

[9]H. C. H. Nip and J. C. Kelly, in *Atomic Collision Phenomena in Solids* (North-Holland, Amsterdam, 1972), p. 50.

[10]L. T. Chadderton, J. Appl. Crystallogr. **3**, 429 (1970).

[11]R. E. De Wames, W. F. Hall, and G. W. Lehman, Phys. Rev. **174**, 392 (1968).

[12]A. Howie, Brookhaven National Laboratory Report No. 50083, 1967 (unpublished).

[13]A. Howie, in *Modern Diffraction and Imaging Techniques in Material Science* (North-Holland, Amsterdam, 1970), p. 295.

[14]A. Howie, M. S. Spring, and P. N. Tomlinson, in *Atomic Collision Phenomena in Solids* (North-Holland, Amsterdam, 1970), p. 34.

[15]J. U. Andersen and W. M. Augustyniak (unpublished).

[16]E. Uggerhøj and F. Frandsen, Phys. Rev. B **2**, 582 (1970).

[17]G. L. Miller and T. Sørensen (unpublished).

[18]R. L. Meek, W. M. Gibson, and R. H. Brown, Nucl. Instrum. Methods **94**, 435 (1971).

[19]A. P. Pogany and P. S. Turner, Acta Crystallogr. A **24**, 103 (1968).

[20]E. Bøgh and J. Whitton, Phys. Rev. Lett. **19**, 553 (1967).

[21]J. U. Andersen and E. Uggerhøj, Can. J. Phys. **46**, 517 (1968).

[22]P. A. Doyle and P. S. Turner, Acta Crystallogr. A **24**, 390 (1968).

[23]C. J. Humphreys and P. B. Hirsch, Philos. Mag. **18**, 115 (1968).

[24]The calculations were performed on the CDC-6400 computer at the University of Aarhus.

[25]L. E. Thomas and C. J. Humphreys, Phys. Status Solidi A **3**, 599 (1970).

[26]M. V. Alain, M. Blackman, and D. W. Pashley, Proc. R. Soc. A **221**, 224 (1954).

[27]F. Frandsen and E. Uggerhøj (unpublished).

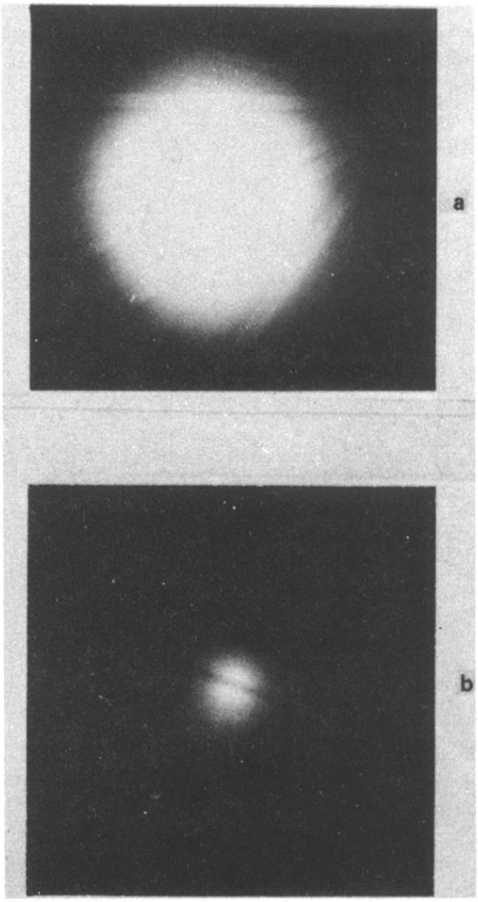

FIG. 12. (a) Photograph showing excess bands in the Rutherford scattering region for a 3200-Å-thick Si crystal. The electron energy was 1.5 MeV; (b) photograph showing a (220) Kikuchi defect band for a 6-μm-thick Si crystal. Electron energy: 1.5 MeV.